Structure of the Surface Vortex Sheet between Two Rotating ^{3}He Superfluids

R. Hänninen,[1] R. Blaauwgeers,[1,2] V. B. Eltsov,[1,3] A. P. Finne,[1] M. Krusius,[1] E. V. Thuneberg,[1,4] and G. E. Volovik[1,5]

[1]*Low Temperature Laboratory, Helsinki University of Technology, P.O. Box 2200, FIN-02015 HUT, Finland*
[2]*Kamerlingh Onnes Laboratory, Leiden University, 2300 RA Leiden, The Netherlands*
[3]*Kapitza Institute for Physical Problems, Kosygina 2, 119334 Moscow, Russia*
[4]*Department of Physical Sciences, University of Oulu, P.O. Box 3000, FIN-90014, Finland*
[5]*Landau Institute for Theoretical Physics, Kosygina 2, 119334 Moscow, Russia*

We study a two-phase sample of superfluid ^{3}He where vorticity exists in one phase (^{3}He-A) but cannot penetrate across the interfacial boundary to a second coherent phase (^{3}He-B). We calculate the bending of the vorticity into a surface vortex sheet on the interface and solve the internal structure of this new type of vortex sheet. The compression of the vorticity from three to two dimensions enforces a structure which is made up of $\frac{1}{2}$-quantum units, independently of the structure of the source vorticity in the bulk. These results are consistent with our NMR measurements.

Consider an interface separating two phases whose order parameters are coherent across the boundary. How do topological line or planar defects behave when they meet the boundary? The coherence rules out simple termination at the interface. The remaining alternatives are that the defect crosses the boundary or is deflected to continue along the boundary. If deflected, how does the defect bend onto the interface and what is its structure when it lies on the boundary? Such questions are certainly relevant for dislocations at coherent grain boundaries in crystals. These questions also appear in liquid crystals [1] and in the cosmos [2,3]. Here we provide an answer in the context of superfluid ^{3}He, where detailed results can be achieved by combining experimental and theoretical analysis [4,5].

The important defects in superfluids are vortex lines or sheets, which can be created in a controlled way by rotation. A crucial property of ^{3}He superfluids are multiple length scales: The core diameter of a typical vortex is 10^3 times larger in the A phase than in the B phase. Correspondingly, the vortex energy in the A phase is lower and vortices do not easily penetrate from the A to the B phase but form a *surface sheet* on the phase boundary (Fig. 1). Here we calculate how the vorticity in bulk ^{3}He-A bends to form such a surface sheet. The calculated internal structure of this surface sheet turns out to be quite different from the vortex sheet that appears in bulk ^{3}He-A. Finally, we report on NMR measurements and show that our calculations are consistent with these.

To obtain a two-phase sample of superfluid ^{3}He, the A-B interface is stabilized in a gradient of magnetic field [5]. Vortices are created by rotating the sample at angular velocity Ω around the axis $\hat{z}$ perpendicular to the interface. In the A-phase section vortices are formed at a low critical velocity v_{cA} so that the average superfluid velocity $\langle v_{sA} \rangle$ approximates solid-body rotation, $\langle v_{sA} \rangle \approx \Omega \times r$. Depending on preparation, the vorticity in the bulk is in the form of vortex lines or vortex sheets [6,7]. Both

structures have a large "soft vortex core" region for which the length scale $\xi_d \sim 10 \ \mu$m is set by weak dipole-dipole forces. The vortex line is doubly quantized in units of the circulation quantum $\kappa_0 = h/2m$, where m is the mass of a ^{3}He atom. The bulk vortex sheet has periodic units, which also consist of two quanta. The B phase vortices, in turn, are singly quantized and have a narrow "hard vortex core" with a radius comparable to the superfluid coherence length $\xi \sim 10$ nm. Their smaller core radius causes the B-phase critical velocity to be at least an order of magnitude larger. Thus, the B phase remains in a metastable vortex-free state, where its superfluid fraction is stationary in the laboratory frame: $v_{sB} = 0$. To sustain the difference in superflow velocities at the A-B interface, the A-phase vorticity has to curve onto the interface where it forms a surface vortex sheet (Fig. 1).

Bending of vorticity into surface sheet.—We calculate the macroscopic configuration for bending the vorticity, in the form of both vortex lines and bulk sheets. For vortex lines we use the Bekarevich-Khalatnikov model [8]. The coarse-grained vorticity $\omega = \frac{1}{2} \nabla \times \langle v_s \rangle$ is determined from the energy functional
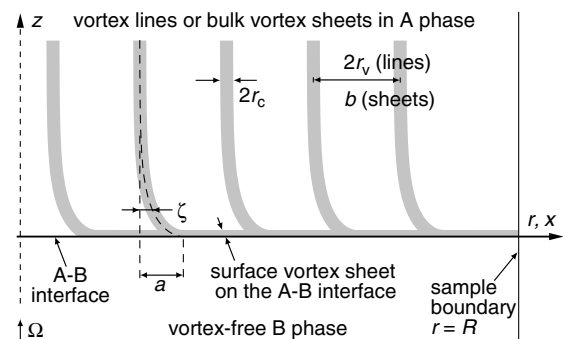

FIG. 1. *A*-phase vorticity (drawn in cross section) curves into a surface vortex sheet on the *A*-*B* interface ($\Omega \sim 1$ rad/s).

$$F = \tfrac{1}{2}\rho_s \int d^3r[\gamma|\boldsymbol{\omega}| + (\langle\boldsymbol{v}_s\rangle - \boldsymbol{v}_n)^2]. \qquad (1)$$

Here ρ_s is the density of the superfluid fraction. The first term is the energy of vortex lines, where $\gamma = (2\kappa_0/\pi)\ln(r_v/r_c)$ (Fig. 1) is on the order of the circulation of a line. The second term is the energy penalty associated with the difference between the average superfluid and normal velocities, $\langle\boldsymbol{v}_s\rangle$ and $\boldsymbol{v}_n = \boldsymbol{\Omega} \times \boldsymbol{r}$. For vortex sheets we use the functional

$$F = \tfrac{1}{2}\rho_s \int d^3r(\boldsymbol{v}_s - \boldsymbol{v}_n)^2 + \int_{\text{sheet}} d^2r\sigma. \qquad (2)$$

The latter term is the surface energy of the bulk sheet, with the surface tension σ. In contrast to Eq. (1), the velocity $\boldsymbol{v}_s = (\hbar/2m)\boldsymbol{\nabla}\phi$ is calculated exactly ($\nabla^2\phi = 0$), treating the bending sheet as a tangential discontinuity of $\boldsymbol{v}_s$.

In rotation with $\boldsymbol{\Omega} = \Omega\hat{\boldsymbol{z}}$, we assume the vorticity to occupy the half space $z > 0$ and not to penetrate to $z < 0$. We select a location far from the axis of rotation so that the cylindrical coordinates can locally be approximated with Cartesian coordinates, taking x in the radial direction. We assume that the vortex sheets at $z \to \infty$ are perpendicular to x [6]. We then find that between two sheets $\boldsymbol{v} = \boldsymbol{v}_s - \boldsymbol{v}_n = 2\Omega(x - c)\hat{\boldsymbol{y}}$, where c is a constant. This allows us to write Eq. (2) as

$$F = \int_0^\infty dz\left[\frac{\rho_s\Omega^2}{6}(b^2 + 12\zeta^2) + \frac{\sigma}{b}\sqrt{1 + \left(\frac{d\zeta}{dz}\right)^2}\right] \qquad (3)$$

Here $b = (3\sigma/\rho_s\Omega^2)^{1/3}$ is the separation of two sheets in the bulk ($z \to \infty$) and ζ is their radial displacement.

Surprisingly, we find that both models [(1) and (3)] give exactly the same form of bending: In spite of different physics and approximations, the radial deviation $\zeta(z)$ of both vortex lines and vortex sheets is given by

$$\frac{z}{a} = 1 - \sqrt{2 - (\zeta/a)^2} - \frac{1}{\sqrt{2}}\ln\frac{\sqrt{2} - \sqrt{2 - (\zeta/a)^2}}{(\sqrt{2} - 1)\zeta/a}. \qquad (4)$$

For vortex lines $a = \sqrt{\gamma/(4\Omega)}$ is on the order of the line spacing $2r_v$. For vortex sheets $a = b/\sqrt{6}$ is 0.41 times their equilibrium spacing in the bulk. The bending contour plotted in Fig. 1 becomes horizontal at the radial deviation $\zeta = a$. After this point the bulk vorticity is transformed to a new state of vortex matter—a surface sheet. The vorticity in the sheet grows linearly with distance r from the center and finally escapes to the vertical sample boundary.

Structure of surface vortex sheet.—The order parameter of superfluid ^{3}He, a 3×3 matrix $A_{\mu j}$, takes in the A phase the form $A_{\mu j} = \Delta_A \hat{d}_\mu(\hat{m}_j + i\hat{n}_j)$. Here $\hat{\boldsymbol{m}}$, $\hat{\boldsymbol{n}}$, and $\hat{\boldsymbol{l}}$ are three orthogonal unit vectors that specify the orbital part of the Cooper pair wave function. The vector $\hat{\boldsymbol{d}}$ specifies the orientation of the spin part. Here we consider only continuous vortex structures where the amplitude Δ_A is constant, and the circulation arises solely from a smooth orientational winding of the triad $(\hat{\boldsymbol{m}}, \hat{\boldsymbol{n}}, \hat{\boldsymbol{l}})$ in space. The vortex textures are determined from the energy functional $F = \int_A d^3r f_A + \int_B d^3r f_B$, where [9]

$$2f_A = \rho_\perp \boldsymbol{v}_A^2 + (\rho_\parallel - \rho_\perp)(\hat{\boldsymbol{l}} \cdot \boldsymbol{v}_A)^2 + 2C\boldsymbol{v}_A \cdot \boldsymbol{\nabla} \times \hat{\boldsymbol{l}} - 2C_0(\hat{\boldsymbol{l}} \cdot \boldsymbol{v}_A)(\hat{\boldsymbol{l}} \cdot \boldsymbol{\nabla} \times \hat{\boldsymbol{l}}) + K_s(\boldsymbol{\nabla} \cdot \hat{\boldsymbol{l}})^2 + K_t(\hat{\boldsymbol{l}} \cdot \boldsymbol{\nabla} \times \hat{\boldsymbol{l}})^2 + K_b|\hat{\boldsymbol{l}}$$
$$\times (\boldsymbol{\nabla} \times \hat{\boldsymbol{l}})|^2 + K_5|(\hat{\boldsymbol{l}} \cdot \boldsymbol{\nabla})\hat{\boldsymbol{d}}|^2 + K_6\sum_{ij}[(\hat{\boldsymbol{l}} \times \boldsymbol{\nabla})_i\hat{d}_j)]^2 + \lambda_d|\hat{\boldsymbol{d}} \times \hat{\boldsymbol{l}}|^2 + \lambda_h(\hat{\boldsymbol{d}} \cdot \boldsymbol{H})^2, \qquad (5)$$

$\boldsymbol{v}_A = \boldsymbol{v}_{sA} - \boldsymbol{v}_n$, and $\boldsymbol{v}_{sA} = (\hbar/2m)\sum_i \hat{m}_i\boldsymbol{\nabla}\hat{n}_i$. The first nine terms give the gradient energy, while the last two terms are the dipole-dipole and external field energies. This functional replaces Eqs. (1) and (2) when the resolution is increased from r_v to the dipolar coherence length $\xi_d = (\hbar/2m)\sqrt{\rho_\parallel/\lambda_d}$. At the A-B interface one has [10]

$$\hat{\boldsymbol{d}} = \overleftrightarrow{R} \cdot \hat{\boldsymbol{s}}, \qquad (\hat{\boldsymbol{m}} + i\hat{\boldsymbol{n}}) \cdot \hat{\boldsymbol{s}} = e^{i\phi}, \qquad \hat{\boldsymbol{l}} \cdot \hat{\boldsymbol{s}} = 0 \qquad (6)$$

as boundary conditions, where $\hat{\boldsymbol{s}}$ is the normal of the interface. The rotation matrix $\overleftrightarrow{R}$ and the phase angle ϕ are quantities appearing in the B-phase order parameter $A_{\mu j} = \Delta_B e^{i\phi}R_{\mu j}$. On the A-phase side the role of the phase angle is played by the rotation angle of $\hat{\boldsymbol{m}}$ and $\hat{\boldsymbol{n}}$ around $\hat{\boldsymbol{l}}$. The boundary conditions (6) imply the coherence of the phase angle across the interface.

We calculate the order parameter in the surface sheet by minimizing the total energy F numerically. The main assumption is that the solutions are homogeneous in the (radial) x direction and periodic in the perpendicular (azimuthal) y direction. Locally these assumptions are

approximately satisfied everywhere except near points where new vorticity enters the sheet. The velocities far above and below the sheet satisfy $|v_B^\infty - v_A^\infty| = 2\kappa_0/L_y$ [or $L_y = 2\kappa_0/(\Omega r)$] when there are two circulation quanta per period L_y. Since the velocity is effectively screened on the A-phase side by vorticity, we can take $v_A^\infty \approx 0$. The experiment is performed in a magnetic field $\boldsymbol{H} \parallel \hat{\boldsymbol{z}}$ which locks $\hat{\boldsymbol{d}} \perp \boldsymbol{H}$ [11]. Since the variation of $\hat{\boldsymbol{d}}$ has only a minor effect, we approximate the B phase $\overleftrightarrow{R}$ with a constant. In contrast, the phase field $\phi(y, z)$ on the B-phase side has to be properly included, via $f_B = \frac{1}{2}\rho_s(\boldsymbol{v}_{sB} - \boldsymbol{v}_n)^2$ and $\boldsymbol{v}_{sB} = (\hbar/2m)\boldsymbol{\nabla}\phi$. Otherwise, a surface vortex sheet is not stable, as is the case for a sheet which would coat a solid container wall [4].

Depending on the density of vorticity in the surface sheet, we obtain two different textures which both incorporate $\frac{1}{2}$-quantum vortex units. These textures are independent of the initial ansatz, i.e., whether a two-quantum vortex line or one period of the bulk vortex sheet is placed above the A-B interface at the start of the iterative energy

minimization. This means that the bulk structures lose their identity and transform at the A-B interface to surface sheet textures.

The low-density texture in Fig. 2 has all the vorticity aligned on the A-B interface. It separates into two composite one-quantum vortices. These consist of two $\frac{1}{2}$-quantum cores, although the vorticity $\nabla \times \boldsymbol{v}_{sA}$ (not shown) cannot be divided into distinct $\frac{1}{2}$-quantum units. At high density a different packing of the vorticity becomes energetically favorable. The resulting texture in Fig. 3 has two $\frac{1}{2}$-quantum cores on the A-B boundary and the remaining circulation localized as a one-quantum vortex above the A-B interface. Here the vorticity $\nabla \times \boldsymbol{v}_{sA}$ is maximized in the $\frac{1}{2}$-quantum regions. The distinguishing feature of the different vortex components is the solid angle which their orientational distribution of $\hat{\boldsymbol{l}}$ covers. For instance, the circular one-quantum vortex above the A-B plane in Fig. 3 includes all orientations of the positive hemisphere with respect to the x axis, while the two $\frac{1}{2}$-quantum vortices each cover one quadrant on the negative hemisphere.

The first-order transition between the two textures takes place at $L_y = 5.7\xi_d$ or when the velocity difference in shear flow $|v_B^\infty - v_A^\infty| \approx 2.8$ mm/s. This value is in the middle of our measuring range. In the calculations the transition is hysteretic, especially on moving from high to low density. Transitions between the two textures are thus expected as a function of Ω and r: The density of the surface vorticity increases with r as $\frac{1}{2}\Omega r/\kappa_0$. Thus, at high Ω one expects to find the low-density texture in the center and the high-density one outside a critical radius.

Transfer of vorticity across A-B interface.—Our NMR measurements of the two-phase sample show that the A-B interface is stable up to high rotation. Ultimately, at a critical angular velocity Ω_c, which corresponds to a critical B-phase superflow velocity $v_c \approx \Omega_c R$ with respect to the container wall at $r \approx R$, the A-B interface undergoes an instability and a small number of circulation quanta manage to cross the interface and form the first vortex lines in the B phase. An analysis of this event as a function of temperature and barrier field shows that v_c is determined by the hydrodynamic rigidity of the interface, on which the texture of the surface vortex sheet has little effect. The upper limit for the density of vorticity in the surface sheet is thus placed by the shear-flow instability. With our solenoidal barrier magnet, this means that $\Omega_c \lesssim 1.6$ rad/s. If the rotation is increased above Ω_c, then the instability occurs repetitively at the constant critical velocity v_c, as analyzed in Fig. 4.

From Fig. 4 it is concluded that the number of circulation quanta ΔN, which is transferred across the A-B interface in one event, can be either odd or even. Measurements accumulated in the constant conditions of Fig. 4 on more than 200 instability events display a smooth probability density distribution $P(\Delta N)$, which is centered around $\langle \Delta N \rangle \approx 8$ and where both odd and even values of ΔN are equally likely. This indicates that the vorticity from the bulk A phase breaks through the A-B interface as single quanta, although the source object, the A-phase vortex, is doubly quantized. Thus, after an instability event the number of quanta in the B-phase section of the sample can be odd, while it is in the bulk A phase even. This means that one unpaired quantum must be accommodated and stored in the surface sheet in stable
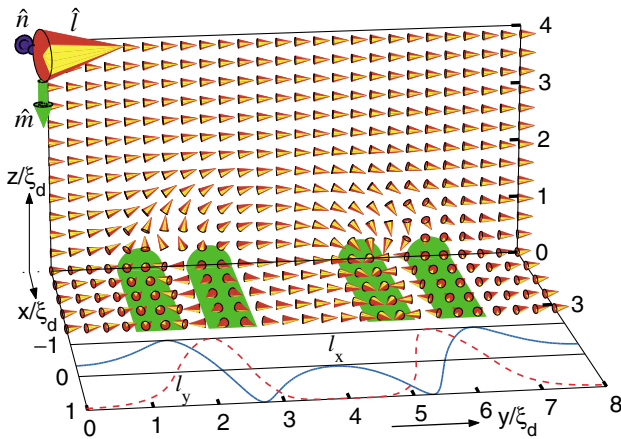

FIG. 2 (color). Orbital texture of the surface sheet at low density of vorticity ($L_y = 8\xi_d$) in a frame where $v_n = 0$. The cones point along $\hat{\boldsymbol{l}}$ and their yellow stripes indicate the rotation of $\hat{\boldsymbol{m}}$ and $\hat{\boldsymbol{n}}$ around $\hat{\boldsymbol{l}}$. On the A-B plane (x-y plane) $\hat{\boldsymbol{l}}$ is parallel to the interface [Eq. (6)]. Its orientations there are shown in the diagram on the bottom. The four highlighted regions ($\hat{\boldsymbol{l}} \approx \pm\hat{\boldsymbol{x}}$) are the centers of $\frac{1}{2}$-quantum cores which pairwise form one-quantum composites. Two $\frac{1}{2}$-quantum cores in one pair are separated by $d_c = 0.26\xi_d + 0.135L_y - 0.0027L_y^2/\xi_d$, when $5.5\xi_d \leq L_y \leq 20\xi_d$.
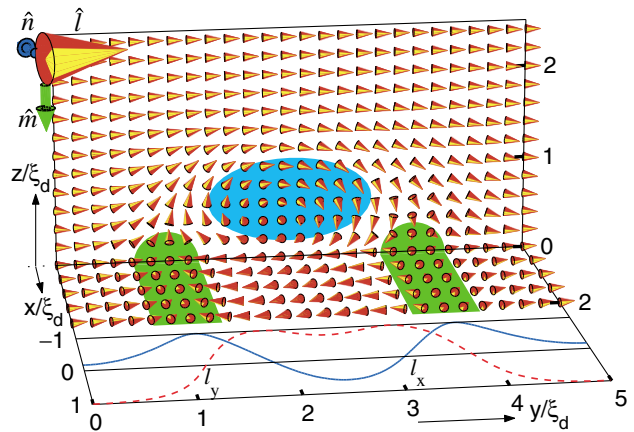

FIG. 3 (color). Orbital texture of the surface sheet at high density of vorticity ($L_y = 5\xi_d$). With increasing density, the two $\frac{1}{2}$-quantum cores in the center of Fig. 2 form a one-quantum composite, a circular *meron*, which pops above the A-B plane, as seen in this figure. The highlighted regions on the A-B plane, the two outermost $\frac{1}{2}$-quantum vortices from Fig. 2, are now isolated, but weakly bound by the meron above the A-B interface. The separation between the $\frac{1}{2}$-quantum cores is $d_c = 0.0743\xi_d + 0.507L_y$, when $2\xi_d \leq L_y \leq 7.5\xi_d$.
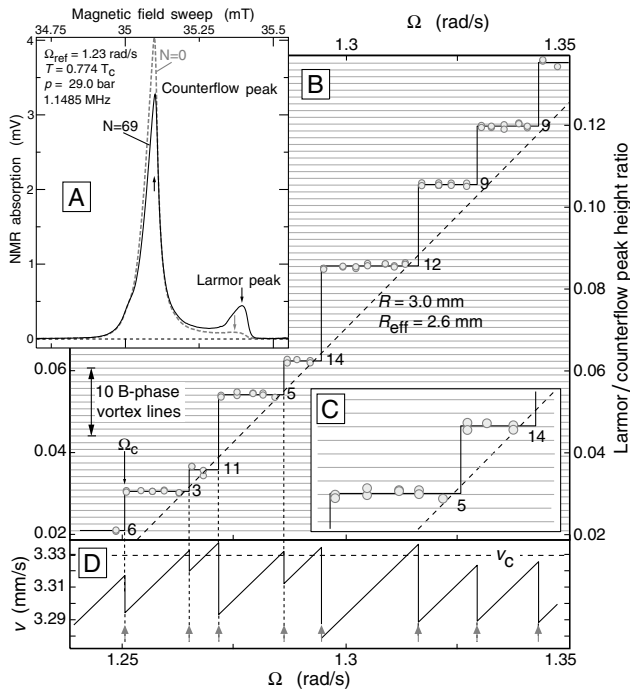
FIG. 4.   NMR measurements on the shear-flow instability of the A-B interface provide information on the A-phase surface vortex sheet. (A) NMR absorption spectra of ^{3}He-B in the vortex-free state ($N = 0$) and with 69 vortex lines ($N = 69$). The ratio of the Larmor and counterflow peak heights, measured at constant conditions (at $\Omega = \Omega_{\rm ref} < \Omega_{\rm c}$), is a linear function of N. (B) A repetitive sequence of instability events with increasing Ω. The data points plot the peak height ratio from NMR spectra measured at $\Omega_{\rm ref}$. The spacing of the horizontal grid lines is the calibrated equivalent of one vortex and yields the number of new B-phase vortex lines ΔN created in each instability event (explicitly given at each discontinuous step). The dashed vertical lines (and arrows in panel D) denote the Ω values where the Larmor peak height rises abruptly while Ω is slowly increased by a small increment. The sloping dashed line is a fit through the corner points and defines the effective radial location $R_{\rm eff}$ of the instability: $N = (2\pi/\kappa_0)R_{\rm eff}^2(\Omega - \Omega_{\rm c})$. (C) One of the instability events in greater detail. The resolution allows us to conclude that ΔN is a small random number, which can be even or odd. (D) Discontinuous superflow velocity with increasing Ω at $r = R_{\rm eff}$: $v = |v_{\rm sB} - v_{\rm n}| = \Omega R_{\rm eff} - \kappa_0 N/(2\pi R_{\rm eff})$. The horizontal dashed line is equivalent to the sloping dashed line in panel B and defines the mean critical velocity $v_{\rm c}$.

state. These properties remain unchanged if the A-phase section of the sample is arranged to support the bulk vortex sheet, in any of its different global configurations, as explained in Ref. [7]. The measurements support the conclusion from the texture calculations that, compared to the bulk A-phase vortex textures, the surface sheet is made up from smaller building blocks and has autonomous structure, independently of the bulk vortex textures above the A-B interface. The experiments cannot as yet distinguish between the two calculated textures, but in

both cases the vorticity can be combined to one-quantum units which allow the transfer of vorticity from the A to the B phase.

Discussion.—Stable vortex sheets are discussed in coherent quantum systems with a multicomponent order parameter. So far, two examples have been experimentally identified, both in anisotropic superfluid ^{3}He-A, namely, the bulk vortex sheet [6] and the present surface sheet. The stability of their structures is based on different principles. The bulk sheet is topologically stable: Its linear quantized vorticity consists of one-quantum building blocks, known as merons or Mermin-Ho vortices, which come pairwise as a combination of a circular and a hyperbolic unit. These are confined within a domain-wall-like planar defect. In the surface sheet the quantized vorticity is confined to two dimensions by the hydrodynamic binding of the circulation to the interfacial boundary. The texture is made up of $\frac{1}{2}$-quantum building blocks to satisfy the in-plane boundary condition of the orbital anisotropy axis $\hat{l}$ at the A-B interface [Eq. (6)]. The two calculated textures are the first with experimental basis, where fractionally quantized units appear in ^{3}He superfluids, since so far the predicted isolated $\frac{1}{2}$-quantum vortex [12] has not been observed in ^{3}He-A.

[1] M. Kleman and O. D. Lavrentovich, *Soft Matter Physics: An Introduction* (Springer-Verlag, Berlin, 2003).
[2] T. W. B. Kibble, in *Topological Defects and Non-Equilibrium Dynamics of Symmetry Breaking Phase Tranitions*, edited by Yu. M. Bunkov and H. Godfrin (Kluwer Academic, Dodrecht, 2000), p. 7.
[3] L. Pogosian and T. Vachaspati, Phys. Rev. D **62**, 105005 (2000); Phys. Rev. Lett. **80**, 2281 (1998).
[4] Ü. Parts *et al.*, Phys. Rev. Lett. **71**, 2951 (1993); Physica (Amsterdam) **197B**, 376 (1994).
[5] R. Blaauwgeers *et al.*, Phys. Rev. Lett. **89**, 155301 (2002); Physica (Amsterdam) **329B–333B**, 57 (2003).
[6] Ü. Parts *et al.*, Phys. Rev. Lett. **72**, 3839 (1994); Physica (Amsterdam) **210B**, 311 (1995).
[7] V. B. Eltsov *et al.*, Phys. Rev. Lett. **88**, 065301 (2002).
[8] I. M. Khalatnikov, *An Introduction to the Theory of Superfluidity* (Benjamin, Inc., New York, 1965), p. 93.
[9] D. Vollhardt and P. Wölfle, *The Superfluid Phases of Helium 3* (Taylor & Francis, London, 1990).
[10] M. C. Cross, in *Quantum Fluids and Solids*, edited by S. B. Trickey, E. D. Adams, and J. W. Duffy (Plenum Press, New York, 1977), p. 183.
[11] At $z \rightarrow +\infty$ outside the soft core regions $\hat{l}$ is homogeneous. This leads to $\hat{l}(z = +\infty) \parallel \hat{y}$. In addition, the coefficients of the functional (5) are evaluated in the weak-coupling approximation at temperatures $T \approx T_{\rm c}$.
[12] M. Salomaa and G. Volovik, Rev. Mod. Phys. **59**, 533 (1987).